World Academy of Science, Engineering and Technology
International Journal of Mechanical and Mechatronics Engineering
Vol:15, No:3, 2021

Numerical Investigation of Developing Mixed Convection in Isothermal Circular and Annular Sector Ducts

Ayad A. Abdalla, Elhadi I. Elhadi, Hisham A. Elfergani

Open Science Index, Mechanical and Mechatronics Engineering Vol:15, No:3, 2021 publications.waset.org/10011918/pdf

***Abstract*—**Developing mixed convection in circular and annular sector ducts is investigated numerically for steady laminar flow of an incompressible Newtonian fluid with $Pr = 0.7$ and a wide range of Grashof number ($0 \le Gr \le 10^7$). Investigation is limited to the case of heating in circular and annular sector ducts with apex angle of $2\phi = \pi/4$ for the thermal boundary condition of uniform wall temperature axially and peripherally. A numerical, finite control volume approach based on the SIMPLER algorithm is employed to solve the 3D governing equations. Numerical analysis is conducted using marching technique in the axial direction with axial conduction, axial mass diffusion, and viscous dissipation within the fluid are assumed negligible. The results include developing secondary flow patterns, developing temperature and axial velocity fields, local Nusselt number, local friction factor, and local apparent friction factor. Comparisons are made with the literature and satisfactory agreement is obtained. It is found that free convection enhances the local heat transfer in some cases by up to 2.5 times from predictions which account for forced convection only and the enhancement increases as Grashof number increases. Duct geometry and Grashof number strongly influence the heat transfer and pressure drop characteristics.

***Keywords*—**Mixed convection, annular and circular sector ducts, heat transfer enhancement, pressure drop.

I. Introduction

THE importance of convective heat transfer in annular and circular sector ducts in many industrial and engineering applications has motivated a significant amount of research. These ducts are encountered for example in multi passage internally finned tubes used in compact heat exchanger applications. Compact heat exchangers frequently involve short passages and hence the flow over the whole or a major part of the heat exchanger is in developing stage [1]. Furthermore, if the flow is laminar, free and forced convection effects are of comparable order of magnitude [2]. Consequently, natural convection and entrance region effects should be considered for better prediction of heat transfer and pressure drop in annular and circular sector duct.

The theme of convective heat transfer in smooth pipe has been extensively studied both theoretically and experimentally for the three limiting thermal boundary conditions; uniform heat flux axially and uniform wall temperature peripherally (H1-thermal boundary condition); uniform heat flux axially and peripherally (H2-thermal boundary condition) and uniform wall temperature axially and peripherally (T-thermal boundary condition). Different theoretical approaches were used to tackle the problem: assuming large Prandtl number, [3]-[5]; using numerical methods [6]-[8]. Experimental studies have also been used to investigate this flow configuration [9]-[13]. Prakash and Liu [14] numerically investigated developing forced convection in internally finned tubes.

Annular and circular sector ducts have received less attention compared to their smooth pipes counterpart. Closed form analytical solutions are rare and can only be obtained in a small number of cases. For flow in semicircular ducts, several studies have been conducted for different flow conditions; developing forced convection [15], fully developed forced convection [16], [17], fully developed mixed convection [18]-[20], fully developed mixed convection in inclined ducts [21], [22] and developing mixed convection for the H1 boundary condition [23]. Experimental and numerical studies on the H1 boundary condition in circular sector ducts of different apex angles have also been reported [24], [25]. Annular sector ducts have also attracted some research interest; forced convection for the friction factor [26] and heat transfer characteristics [27], and fully developed flow for both the Hl and H2 boundary analytically [28] and numerically [29]. Radiation-affected laminar natural convection in the cylindrical annuli [30] and developing mixed convection in horizontal concentric annulus [31] have been investigated as well. Some studies focused on the influence of other physics on heat transfer and pressure drop in annular and circular such as the presence of porous medium, [32]-[39]; nanofluids, [40]-[42] and non-Newtonian effects [43], [44].

The objective of this study is to investigate the developing steady laminar mixed convection in horizontal annular and circular sector ducts with constant wall temperature. The effect of duct geometry on heat transfer and pressure drop will be studied at different values of Grashof number using the SIMPLER algorithm which is a control volume finite difference based method for solving coupled partial differential equations.

II. Mathematical Formulation

The current focus is the developing mixed convection in isothermal annular and circular sector ducts. The flow is steady and laminar with negligible axial conduction and viscous dissipation. The fluid is Newtonian and

A. A. Abdalla is with the Department of Mechanical Engineering, University of Benghazi, Benghazi, Libya (corresponding author, phone: +218922192935; e-mail: Ayad.abdalla@uob.edu.ly).

H. A. Elfergani and E. I. Elhadi are with the Department of Mechanical Engineering, University of Benghazi, Benghazi, Libya (e-mail: Hisham.elfergani@uob.edu.ly, Elhdi_elhdi@yahoo.com).

Open Science Index, Mechanical and Mechatronics Engineering Vol:15, No:3, 2021 publications.waset.org/10011918/pdf

incompressible with constant properties except for density which is assumed to be temperature dependent (Boussinesq approximation) in formulating the body force terms. The geometry under consideration and the coordinate system is shown in Fig. 1. The duct has an inner radius of r_i, an outer radius of r_o, and an opening angle of 2ϕ and is orientated at an angle of γ from the vertical axis and inclined by an angle equals to α to the horizontal axis. The fluid enters the duct with a uniform velocity and temperature of u_b and t_e, respectively. The temperature of the wall of the duct is assumed constant at any cross section of the duct and equals to, t_w. The fluid pressure decomposition [45] is used to parabolize the elliptic Navier-Stokes equations. This step enables the use of the marching technique to advance the solution in the axial direction. The pressure is divided into two parts, the first is a function of the axial location only and it is the driving force of the main flow while the second is a function of angular and radial coordinates only and it is the driving force of the secondary flow. The two parts are independent of each other and can be written as:

$$p(x,r,\theta) = \bar{p}(x) + p'(r,\theta) \tag{1}$$

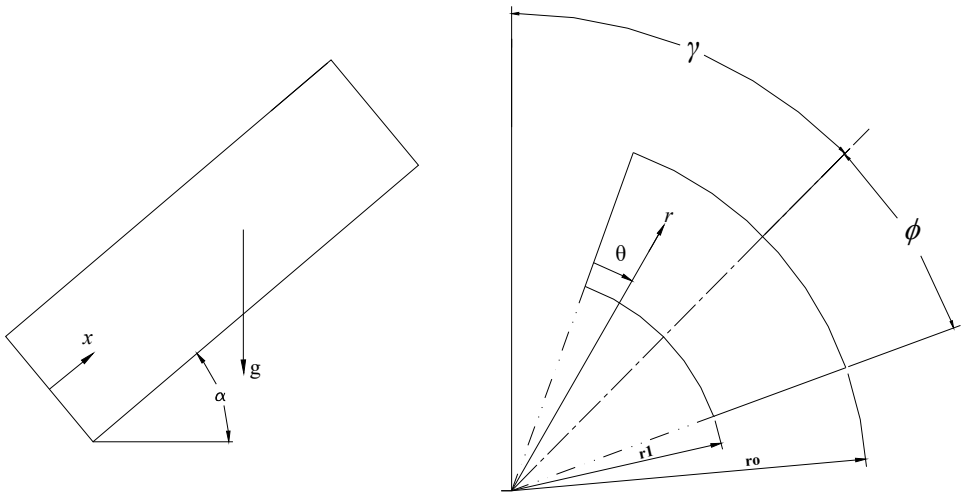

Fig. 1 Geometry and coordinates under consideration

The governing Navier-Stokes equations and the energy equation in cylindrical coordinates can be written in a non-dimensional form using the following set of non-dimensional parameters:

$$\left.\begin{aligned} &R=\frac{r}{r_o},\ X=\frac{x/d}{Re\,Pr},\ U=\frac{u}{u_b},\ V=\frac{vd}{\nu},\ W=\frac{wd}{\nu},\ T=\frac{t-t_w}{t_e-t_w}\\ &P'=\frac{gd^2}{\nu^2}r\cos(\theta+\gamma-\varphi)+\cos\alpha+\frac{p'd^2}{\rho\nu^2},\ \ \bar{P}=\frac{g}{u_b{}^2}x\sin\alpha+\frac{\bar{p}}{\rho u_b^2}\\ &Re=\frac{u_b d}{\nu},\ Pr=\frac{\mu c_p}{k},\quad Gr=\frac{gd^3\beta(t_w-t_e)}{\nu^2}\end{aligned}\right\} \tag{2}$$

The non-dimensional governing equations become:
Continuity equation

$$\frac{\partial(RV)}{\partial R}+\frac{\partial W}{\partial\theta}+\frac{R}{2Pr}\frac{\partial U}{\partial X}=0 \tag{3}$$

Axial momentum equation:

$$V\frac{\partial U}{\partial R}+\frac{W}{R}\frac{\partial U}{\partial\theta}+\frac{1}{2Pr}U\frac{\partial U}{\partial X}=-\frac{1}{2Pr}\frac{d\bar{P}}{dX}-\frac{Gr}{Re}\frac{T}{2}\sin\alpha\ + 2\left[\frac{1}{R}\frac{\partial}{\partial R}\left(R\frac{\partial U}{\partial R}\right)+\frac{1}{R^2}\frac{\partial^2 U}{\partial\theta^2}\right] \tag{4}$$

Radial momentum equation:

$$V\frac{\partial V}{\partial R}+\frac{W}{R}\frac{\partial V}{\partial\theta}+\frac{1}{2Pr}U\frac{\partial V}{\partial X}= -\frac{\partial P'}{\partial R}+2\left[\frac{\partial}{\partial R}\left(\frac{1}{R}\frac{\partial(RV)}{\partial R}\right)+\frac{1}{R^2}\frac{\partial^2 V}{\partial\theta^2}+\frac{W^2}{R}-\frac{2}{R^2}\frac{\partial W}{\partial\theta}\right]- \frac{Gr}{2}T\cos\alpha\cos(\theta+\gamma-\varphi) \tag{5}$$

Angular momentum equation:

$$V\frac{\partial W}{\partial R}+\frac{W}{R}\frac{\partial W}{\partial\theta}+\frac{1}{2Pr}U\frac{\partial W}{\partial X}= -\frac{\partial P'}{\partial\theta}+2\left[\frac{\partial}{\partial R}\left(\frac{1}{R}\frac{\partial(RW)}{\partial R}\right)+\frac{1}{R^2}\frac{\partial^2 W}{\partial\theta^2}-\frac{VW}{R}+\frac{2}{R^2}\frac{\partial V}{\partial\theta}\right]+ \frac{Gr}{2}T\cos\alpha\sin(\theta+\gamma-\varphi) \tag{6}$$

Energy equation:

$$\frac{Pr}{2}\left[V\frac{\partial T}{\partial R}+\frac{W}{R}\frac{\partial T}{\partial\theta}+\frac{1}{2Pr}U\frac{\partial T}{\partial X}\right]=\frac{1}{R}\frac{\partial}{\partial R}\left(R\frac{\partial T}{\partial R}\right)+\frac{1}{R^2}\frac{\partial^2 T}{\partial\theta^2} \tag{7}$$

$U(X,R,\theta)$, $V(X,R,\theta)$, $W(X,R,\theta)$ are the non-dimensional velocity components in the X-, R- and θ-directions, respectively, $T(X,R,\theta)$ is the dimensionless fluid temperature.

The applicable initial and boundary conditions are:

$$\left.\begin{aligned} &\text{For } X=0:\\ &\quad U=T=0 \quad \text{at all solid boundaries}\\ &\quad U=T=1,\ \bar{P}=\bar{P}_o \quad \text{for } R_1<R<1 \text{ and } 0<\theta<2\varnothing\\ &\quad V=W\ P'=0 \quad \text{for } R_1\le R\le 1 \text{ and } 0\le\theta\le 2\varnothing\\ &\text{For } X>0:\\ &\quad U=V=W=T=0 \quad \text{at all solid boundaries,}\\ &\text{where } R_1=r_i/r_o\end{aligned}\right\} \tag{8}$$

Open Science Index, Mechanical and Mechatronics Engineering Vol:15, No:3, 2021 publications.waset.org/10011918/pdf

Some important parameters are calculated after solving the governing equations, such as Nusselt number, the product *fRe*, and the product $f_{app}Re$.

Local friction factor is calculated from the peripherally averaged shear stress as:

$$f = \frac{\overline{\tau}_w}{\left(\frac{1}{2}\rho u_b^2\right)} \tag{9}$$

The product *fRe* is then calculated from:

$$fRe = \frac{2\varphi(1-R_1^2)}{[\varphi+1+R_1(\varphi-1)]^2}\left[\int_{R_1}^{1}\left(\frac{\partial U}{R\partial\theta}\right)_{\theta=0}dR + \int_0^{2\varphi}\left(\frac{\partial U}{\partial R}\right)_{R=R_1}R_1 d\theta - \int_{R_1}^{1}\left(\frac{\partial U}{R\partial\theta}\right)_{\theta=2\varphi}dR - \int_0^{2\varphi}\left(\frac{\partial U}{\partial R}\right)_{R=1}d\theta\right] \tag{10}$$

In the entrance region of the duct, the pressure drop is attributed to two effects; the surface shear forces and the increase in the total fluid momentum flux resulting from the development of the velocity profile. A single apparent mean friction factor, f_{app} which combines both effects [46] is calculated for horizontal ducts from:

$$f_{app} = d_h\frac{(\overline{p}_o-\overline{p})/x}{(2\rho u_b^2)} \tag{11}$$

Then the product $f_{app}Re$ is given by:

$$f_{app}Re = -\left[\frac{\varphi(1-R_1^2)}{(\varphi+1)+R_1(\varphi-1)}\right]^2\frac{1}{2Pr}\left[\frac{\overline{P}-\overline{P}_o}{X}\right] \tag{12}$$

The circumferentially averaged Nusselt number, ($Nu = hd_h/k$), is calculated as:

$$Nu = \frac{\varphi(1-R_1^2)}{[\varphi+1+R_1(\varphi-1)]^2T_b}\left[\int_{R_1}^{1}\left(\frac{\partial T}{R\partial\theta}\right)_{\theta=0}dR + \int_0^{2\varphi}\left(\frac{\partial T}{\partial R}\right)_{R=R_1}R_1 d\theta - \int_{R_1}^{1}\left(\frac{\partial T}{R\partial\theta}\right)_{\theta=2\varphi}dR - \int_0^{2\varphi}\left(\frac{\partial T}{\partial R}\right)_{R=1}d\theta\right] \tag{13}$$

The bulk temperature is calculated from:

$$T_b = \frac{1}{\varphi(1-R_1^2)}\int_0^{2\varphi}\int_{R_1}^{1}UTR\partial R\partial\theta \tag{14}$$

III. Solution Procedure and Accuracy Assessment

A. Solution Procedure

The governing equations, subject to the attendant boundary conditions, are solved numerically using a control volume based finite difference method. The governing equations are discretized on a staggered grid and the power law scheme [47] is used for the treatment of convection and diffusion terms. The mesh has uniform divisions in the radial and angular directions and non-uniform divisions in the axial direction. The control volumes adjacent to solid walls are subdivided into two subdivisions in order to capture the steep gradient in the velocity and temperature, while in the axial direction, small values of increment, ΔX, are used near the duct inlet, increasing gradually in the main flow direction up to a maximum value which is then kept constant. Fig. 2 shows the mesh used in this study.

The SIMPLER algorithm [47] is used in handling the resulting system of equations. The continuity equation is used to construct pressure and pressure correction equations. The pressure equation is employed to generate a pressure distribution which is used to solve radial and angular momentum equations. The pressure correction equation, on the other hand, is used to correct the computed radial and angular velocities to satisfy continuity equation and eventually, axial momentum equation and energy equation are solved.

The solution is carried out in the developing region using the marching technique in the axial direction starting at the entrance and progressing in the direction of main flow until the flow is fully developed.

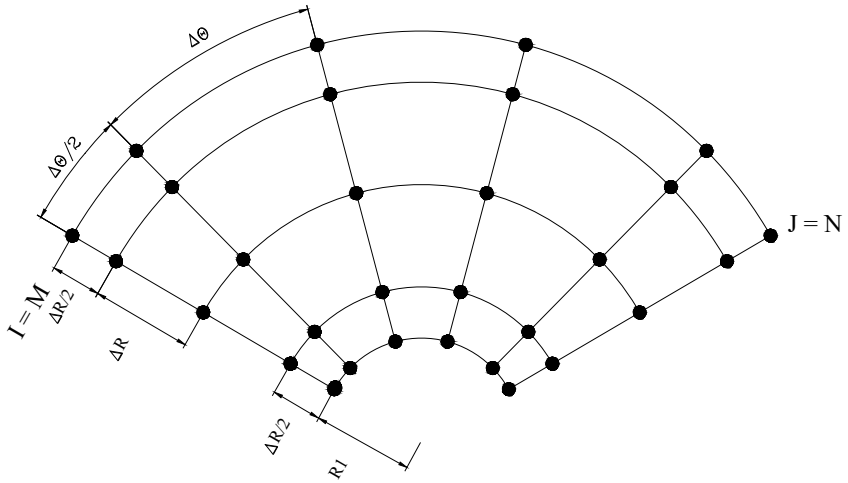

Fig. 2 Grid map and computational domain

The discretized equations are solved for each radial line using the tri-diagonal matrix algorithm (TDMA), and the solution domain was covered by double sweeping line by line in the angular direction. Iterations continue until the relative

Open Science Index, Mechanical and Mechatronics Engineering Vol:15, No:3, 2021 publications.waset.org/10011918/pdf

change of *U, V, W* and T is within ± 10^{-3}% and the absolute value of the continuity equation residual is less than 10^{-5}. A computer code is written in FORTRAN programming language to perform these computations.

The selection of the mesh size in the radial and angular directions is guided by the accuracy of the results of the fully developing *fRe* and *Nu* at zero Grashof number for the semicircular duct geometry, Table I. Based on these results, a mesh of 30×40 (Radial × Angular) subdivisions is selected as a reasonable compromise between computer time and accuracy.

TABLE I
SELECTION OF MESH SIZE

Mesh Size (R×θ)	30×20	30×30	30×40	30×50	30×60	40×40	50×40
Nu	3.335	3.325	3.323	3.322	3.321	3.320	3.320
f Re	15.651	15.717	15.739	15.750	15.755	15.754	15.761

Several numerical experimentations are conducted in order to determine the appropriate axial step size. Based on the accuracy of the results in the developing region for the forced convection in semicircular duct, the following scenario is adopted for ΔX: the first axial step equals to 10^{-5} increasing gradually by a factor of 5% to a maximum $\Delta X = 10^{-3}$, then it is kept constant up to $X = 0.20$ which is far enough to be considered fully developed

B. Validation of Accuracy

The computer program developed in this study has been successfully validated by comparing the predicted results with those from previous analytical and numerical studies for limiting cases available in the literature. Table II shows comparisons of the present results to previous results of pure forced convection for different combinations of the geometrical parameters R_1 and 2ϕ. These comparisons indicate good agreement between the present and previous results.

TABLE II
RESULTS VALIDATION FOR $Pr = 0.7$, $Gr = 0$

Geometry		$R_1 = 0$, $2\phi = \pi/4$	$R_1 = 0$, $2\phi = \pi/3$	$R_1 = 0$, $2\phi = \pi$	$R_1 = 0.5$, $2\phi = \pi 2$	$R_1 = 0.5$, $2\phi = 2\pi 3$
f Re	present	13.744	14.171	15.739	16.091	17.188
	previous	13.660▲	14.200*	15.790*	16.163*	17.273*
	% deviation	0.61	-0.20	-0.32	-0.45	-0.49
Nu	present	2.626	2.801	3.323	3.572	3.988
	previous	2.643▲	2.822*	3.316*	3.562*	3.966*
	% deviation	-0.64	-0.74	0.21	0.28	0.55

(▲:Ref. [14], *: Ref. [29])

IV. RESULTS AND DISCUSSION

The results are obtained in the developing region of flow in circular ducts having apex angle of π/4 for $Pr = 0.7$ and $0 \leq Gr \leq 10^7$. Comparisons are made between circular sector duct ($R_1 = 0$) and annular sector duct of $R_1 = 0.5$ in terms of the secondary flow, axial velocity field and temperature distribution as well as local averaged variable such as *fRe*, $f_{app}Re$, and *Nu*. Although, duct orientation and inclination are included in the formulation and computer code, it is decided to limit results to horizontal ducts with zero orientation in the current study. The hydrodynamic and thermal development of the flow is presented in terms of velocity and temperature contour lines as well as secondary flow pattern at the highest value of Grashof number ($Gr = 10^7$) where the effect of free convection is more pronounced. Finally, the local averaged parameters, *fRe*, $f_{app}Re$, and *Nu* are presented for different *Gr* values.

A. Secondary Flow Pattern

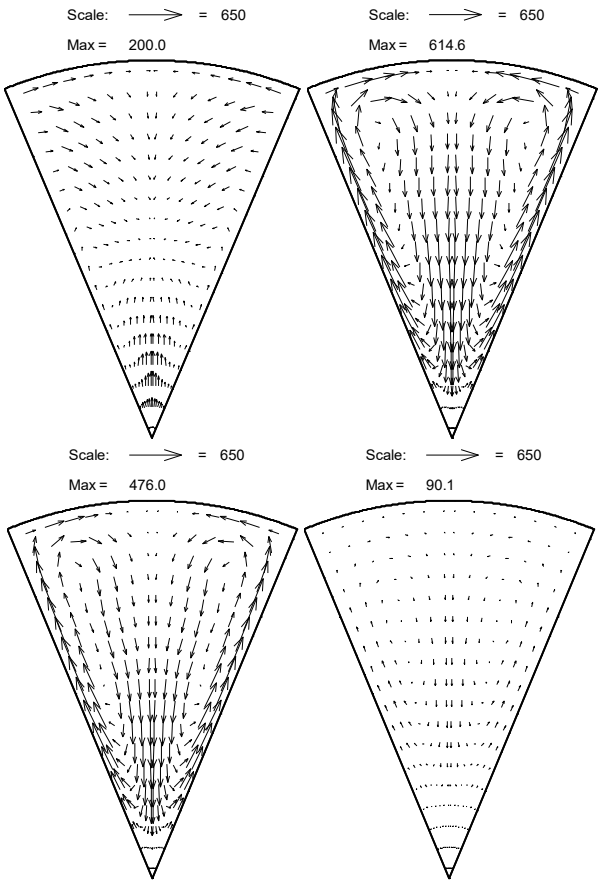

Fig. 3 Development of secondary flow pattern ($Gr = 10^7$, $R_1 = 0$)

The growth and decay of secondary flow along the duct axis for circular sector duct are shown in Fig. 3. Four axial location corresponding to X = 10^{-4}, 10^{-3}, 1.93 ×10^{-3} (the location where *Nu* is peak) and 10^{-2} are presented. In developing mixed convection flow through isothermal ducts, a secondary flow field is generated due to two effects, the boundary layer mass displacement effect and the buoyancy effect. Entrance effect dominates the flow in the region near the duct inlet making the secondary flow field resembles that of pure forced convection. Thus, the flow moves the fluid from the retarding areas near the walls to the accelerating areas in the duct core. Further downstream, the buoyancy effect appears and becomes dominant which makes the warmer fluid near the solid walls moves upward generating two rotating secondary flow cells.

Hot fluid moves up along the flat walls, deflected by the curved wall towards the middle of the curved wall and then descends in the central part of the duct. Further downstream,

the intensity of secondary flow increases to a maximum value and then decreases until it diminishes in the fully developed region as the bulk temperature approaches the wall temperature.

The overall trend of growing and then decaying secondary flow is observed for the flow in annular sector ducts as well. However, different behavior is noticed, the upward curvature of the inner curved wall trigger the formation of two additional secondary flow cells as shown in Fig. 4. Two large counter rotating cells appear in the upper part with upward flow along the flat walls and outer curved wall and another two smaller counter rotating cells emerge in the lower part with upward flow along the lower curved wall. As the flow proceeds, the intensity of the secondary flow increases to maximum and then decreases gradually until it disappears in the fully developed region.

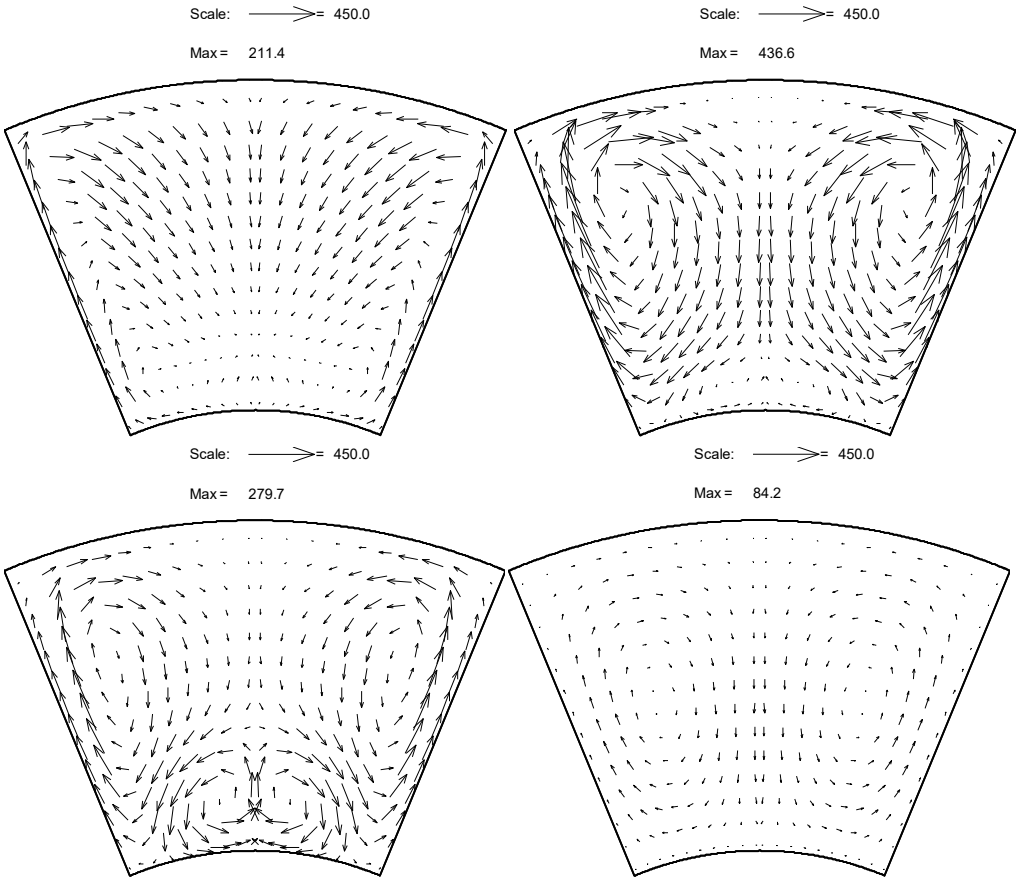

Fig. 4 Development of secondary flow pattern ($Gr = 10^7$, $R_1 = 0.5$)

B. Axial Velocity Field

The disparity between the secondary flow patterns of circular and annular sector ducts is reflected in their axial velocity and temperature distributions. Fig. 5 shows the axial velocity distributions for flow in the circular sector duct at the axial locations stated above in addition to the fully developed case ($X = 0.2$). Near duct inlet where buoyancy effects are negligible, velocity contours are less disturbed and steep velocity changes take place in the proximity of solid walls with the velocity is constant in most of duct cross section. As the flow proceeds, distortion to the velocity contours due to free convection effect is noticed mainly in the top region of the cross-section and the maximum velocity is observed in single location. The maximum velocity increases in magnitude and shifts downward along the symmetry line compressing the contours at the lower region. Finally, as the flow reaches fully developed region, the location of maximum axial velocity moves up towards the middle of the duct cross section and its value increases to $U_{max} = 2.193$. On the other hand, the development of axial velocity for the flow in annular sector ducts reveals the formation of two maximum velocity regions near the bottom curved wall as shown in Fig. 6. At the duct entrance the maximum velocity noticed at single location. As the fluid moves away from the inlet, the axial contours are distorted by the buoyancy effect. The distortion first appears in the top region of the cross-section whereas a slight distortion is noticed in the bottom region. Further downstream, the distortions are noticed in the top and bottom regions with two maximum velocity regions in the cooler fluid core near the bottom curved wall due to the presence of four secondary flow cells. As the fluid proceeds, the distortions of the axial velocity contours disappear and finally these contours tend to attain the fully developed situation. In the fully developed region entrance and buoyancy effects

Open Science Index, Mechanical and Mechatronics Engineering Vol:15, No:3, 2021 publications.waset.org/10011918/pdf

diminish and then the axial velocity distribution is similar to that of fully developed forced convection which consists of symmetric closed loops (along the duct symmetry line) and single maximum axial velocity existed at the middle of the duct ($U_{max} = 2.085$).

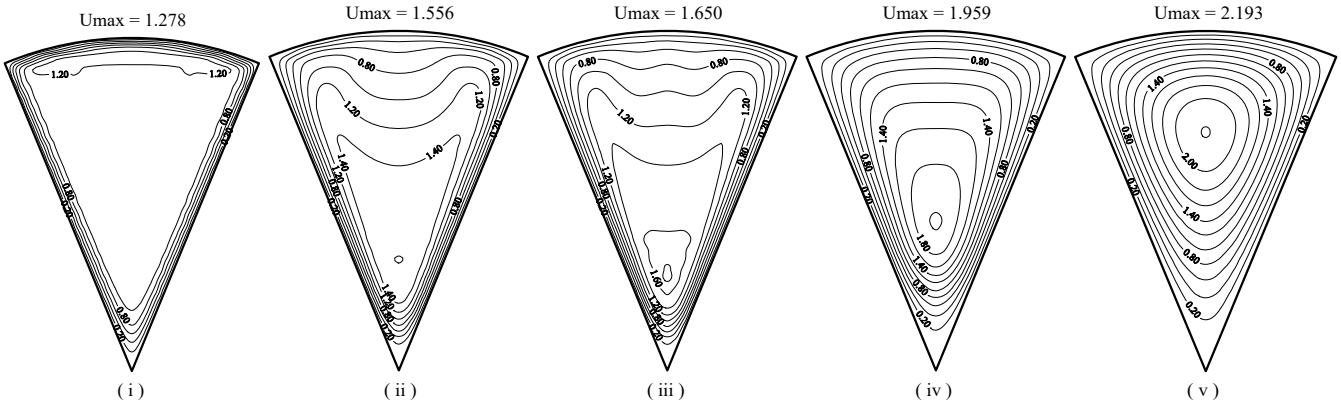

Fig. 5 Development of axial velocity, (Gr=10^7, R_1=0)

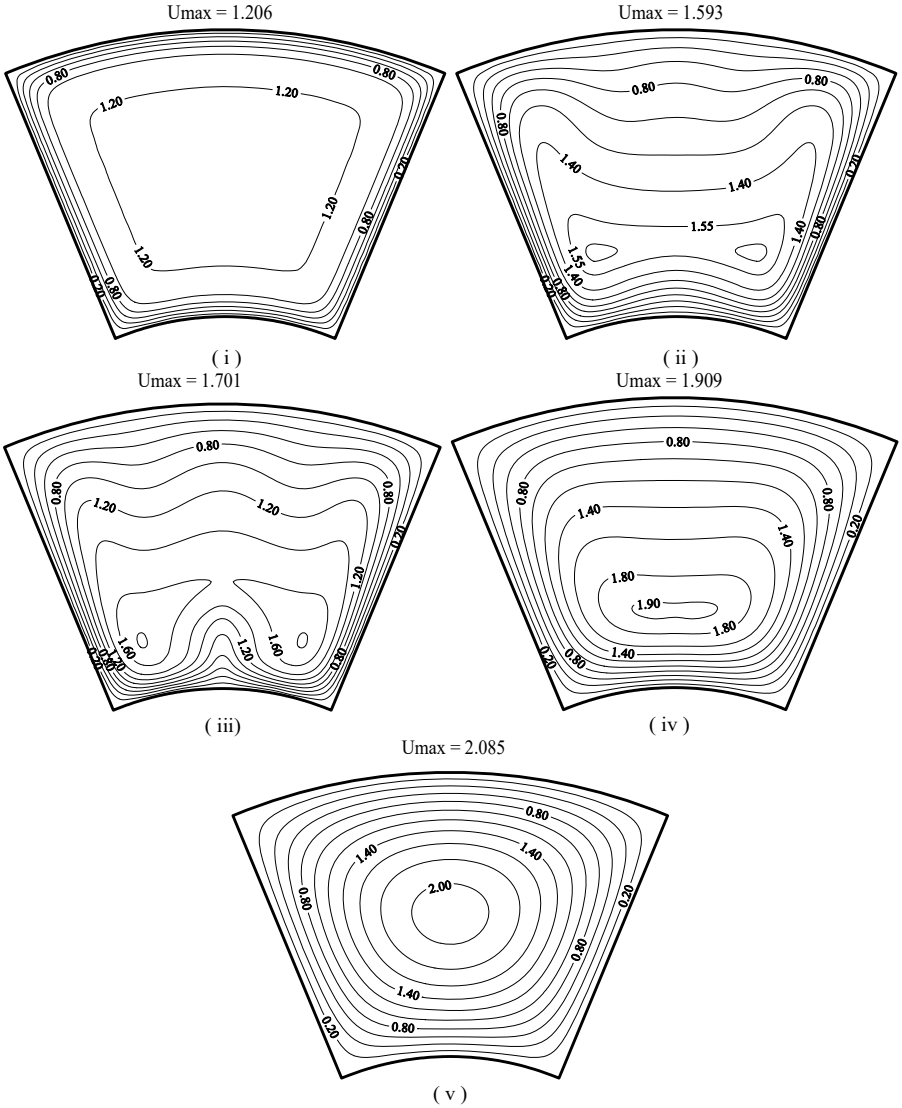

Fig. 6 Development of axial velocity (Gr = 10^7, R_1 = 0.5)

Open Science Index, Mechanical and Mechatronics Engineering Vol:15, No:3, 2021 publications.waset.org/10011918/pdf

Open Science Index, Mechanical and Mechatronics Engineering Vol:15, No:3, 2021 publications.waset.org/10011918/pdf

C. Temperature Distribution

The development of temperature field in terms of contours of (T/T_b) for the considered geometries at $Gr = 10^7$ are presented in Figs. 7 and 8. Near the duct entrance, the isotherms are represented by concentric closed loops approximately equally spaced near the wall except at corners. Further downstream, the isotherms are distorted as a result of buoyancy effects.

For the circular sector duct, Fig. 7, the isotherms are distorted at the top region and the maximum (T/T_b) is shifted downwards resulting in closely spaced contours at the lower region and sparsely spaced contours at the upper region. The maximum (T/T_b) is observed only in one location in the duct cross-section on its symmetry line. As the flow proceeds, the distortion of the temperature contours is reduced and the maximum (T/T_b) is shifted upward along the symmetry line towards the duct center with $(T/T_b)_{\max} = 1.944$ in the fully developed region. Similar trend is observed in Fig. 8 for the flow in annular sector ducts. However, two maxima are noticed as a result of four-cell secondary flow shown in Fig. 4. As the flow advances, the value $(T/T_b)_{\max}$ first increases and then decreases to $(T/T_b)_{max} = 1.854$ in the fully developed region.

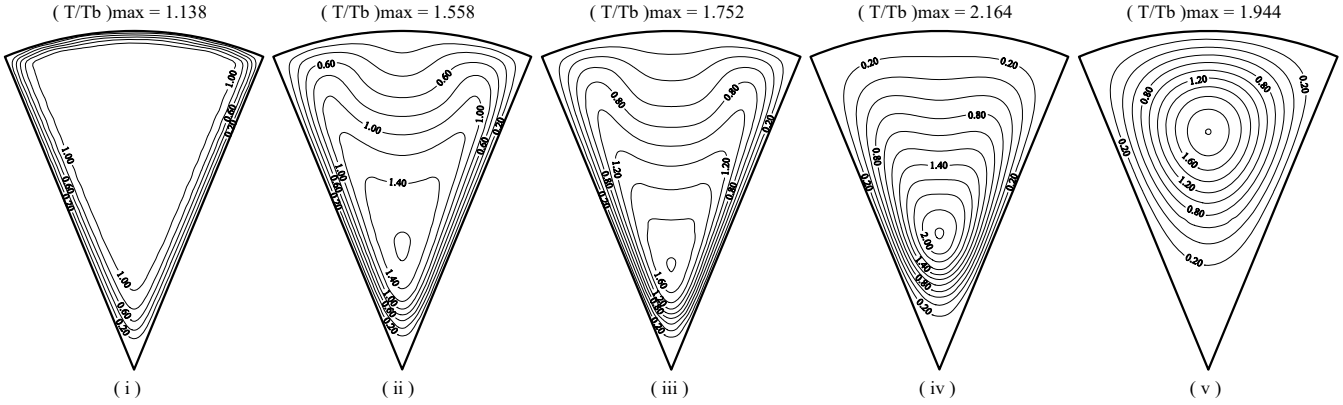

Fig. 7 Development of temperature distribution ($Gr = 10^7$, $R_1 = 0$)

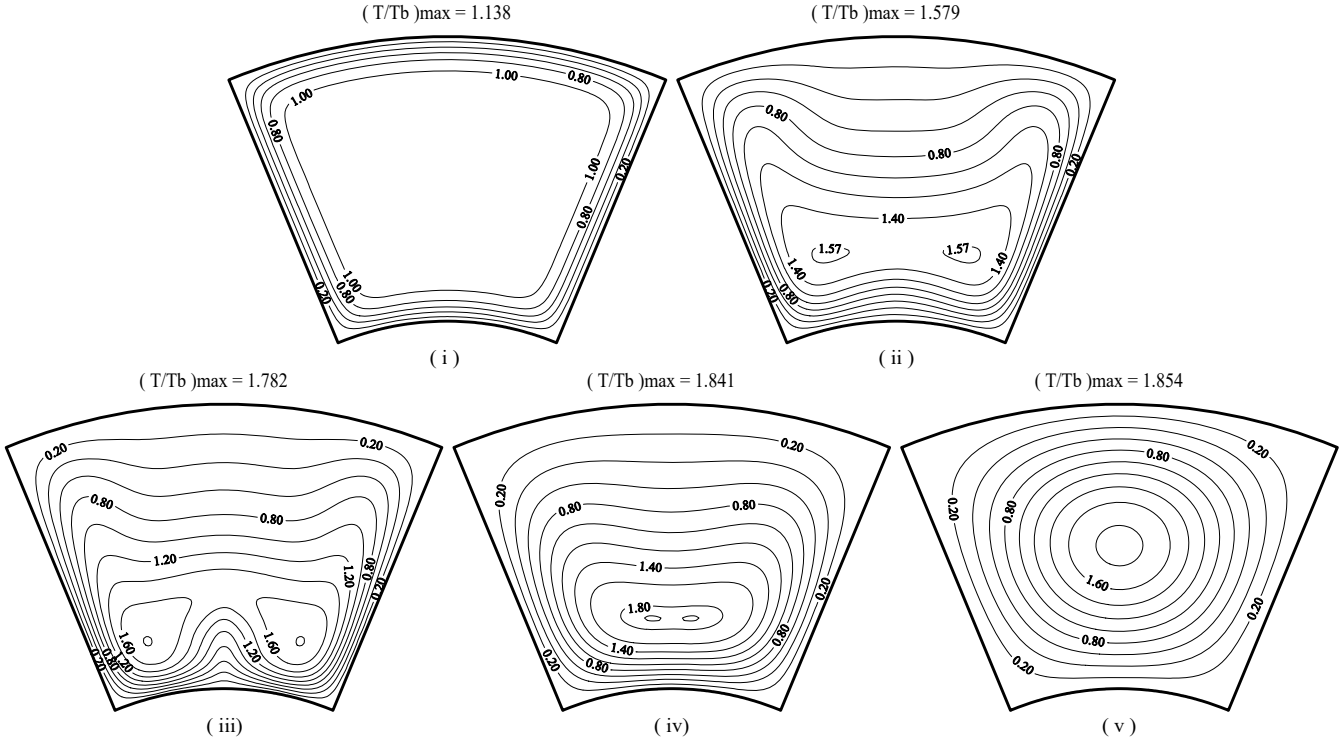

Fig. 8 Development of temperature distribution ($Gr = 10^7$, $R_1 = 0.5$)

D. Local Nusselt Number and Friction Factor

Fig. 9 shows effect of Grashof number on the local parameters *Nu, fRe, NU/fRe* and $f_{app}Re$ for circular sector. Near the inlet, since the free convection effects are insignificant, all the curves follow the pure forced convection curve. As the flow proceeds downstream, the buoyancy forces

become significant and mixed convection curves rise above the pure forced convection curves. The increase in Nu becomes appreciable at $Gr \geq 10^6$ owing to the strong buoyancy effect. Increasing Grashof number decreases the entrance length prior to onset of marked free convection and increases Nu_{max} and shifts its location toward the duct inlet. It should be noted that this location roughly corresponds to the axial location where the secondary flow most vigorous. Nusselt number then gradually decreases until reaches a practically constant value of *2.6256* which corresponds to the fully developed forced convection value, Fig. 9 (a).

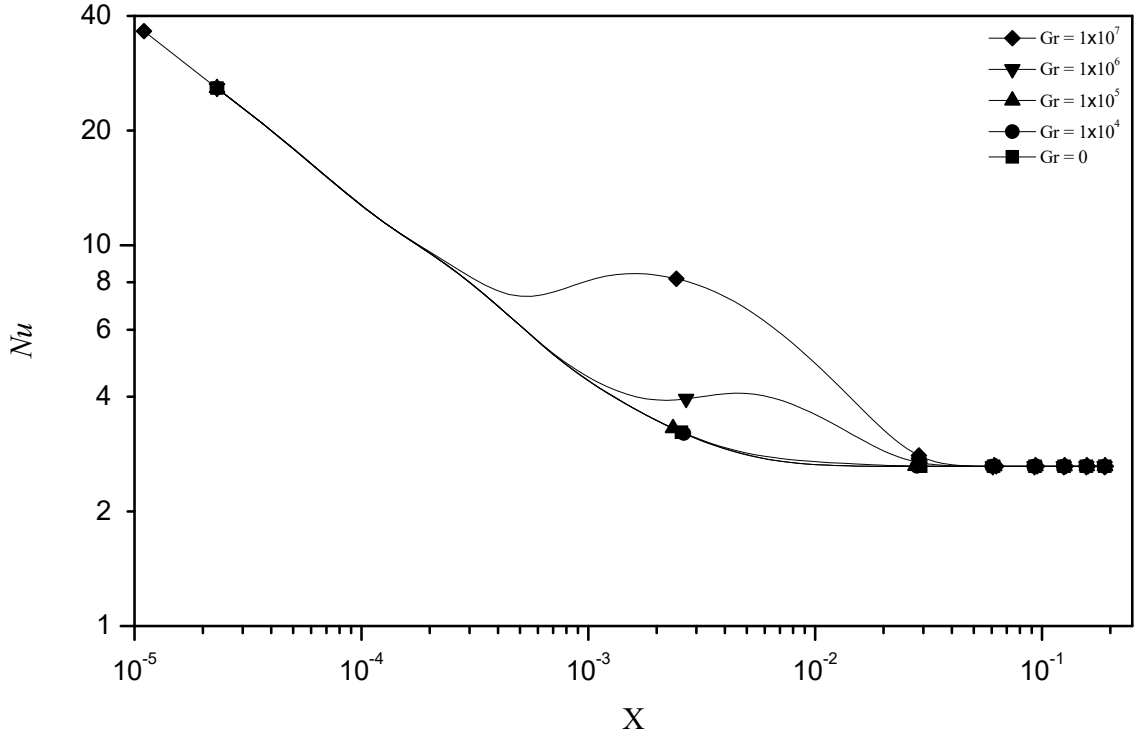

(a)

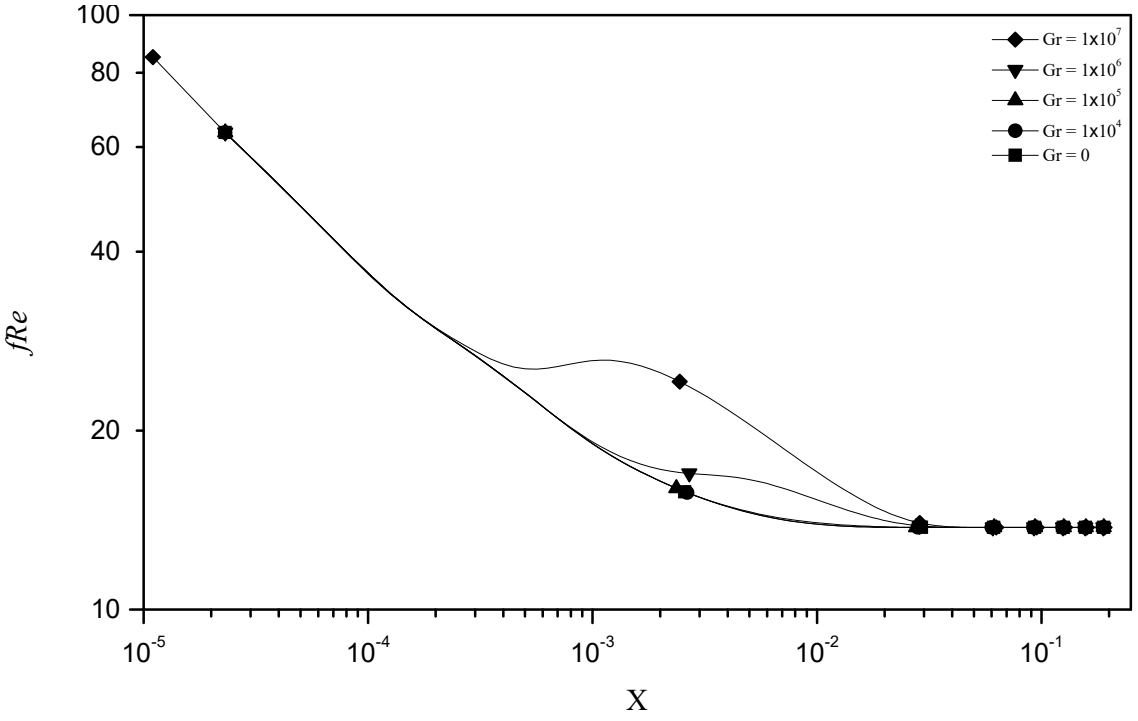

(b)

Open Science Index, Mechanical and Mechatronics Engineering Vol:15, No:3, 2021 publications.waset.org/10011918/pdf

Open Science Index, Mechanical and Mechatronics Engineering Vol:15, No:3, 2021 publications.waset.org/10011918/pdf

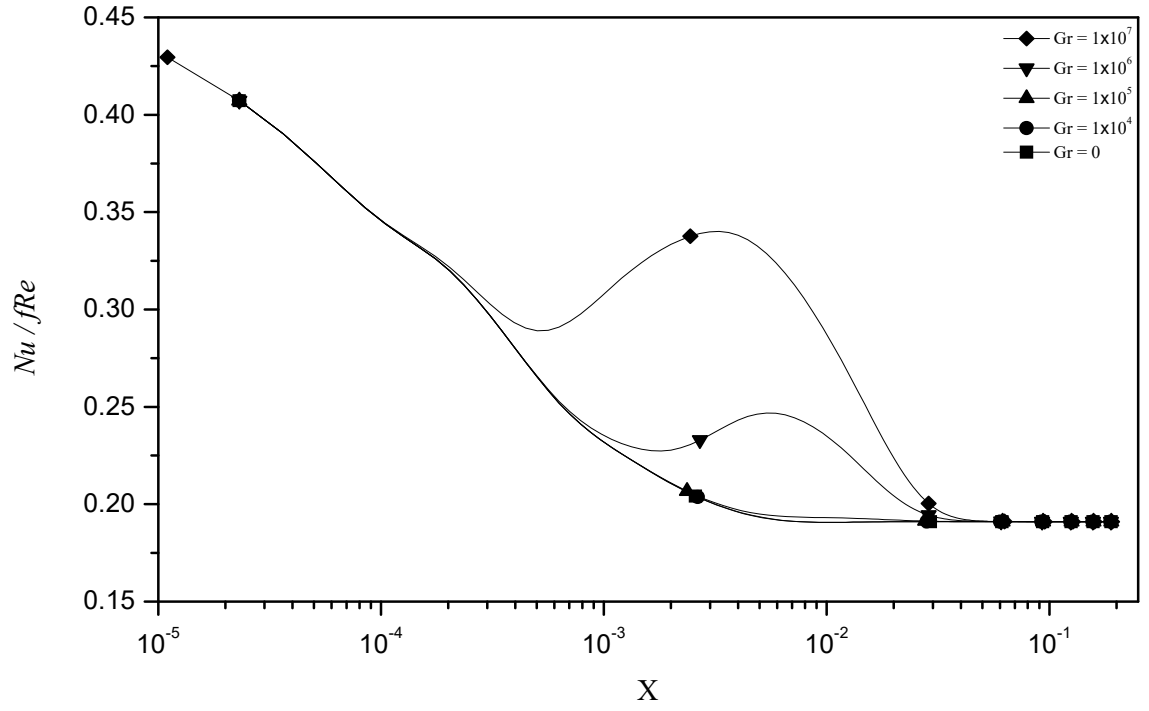

(c)

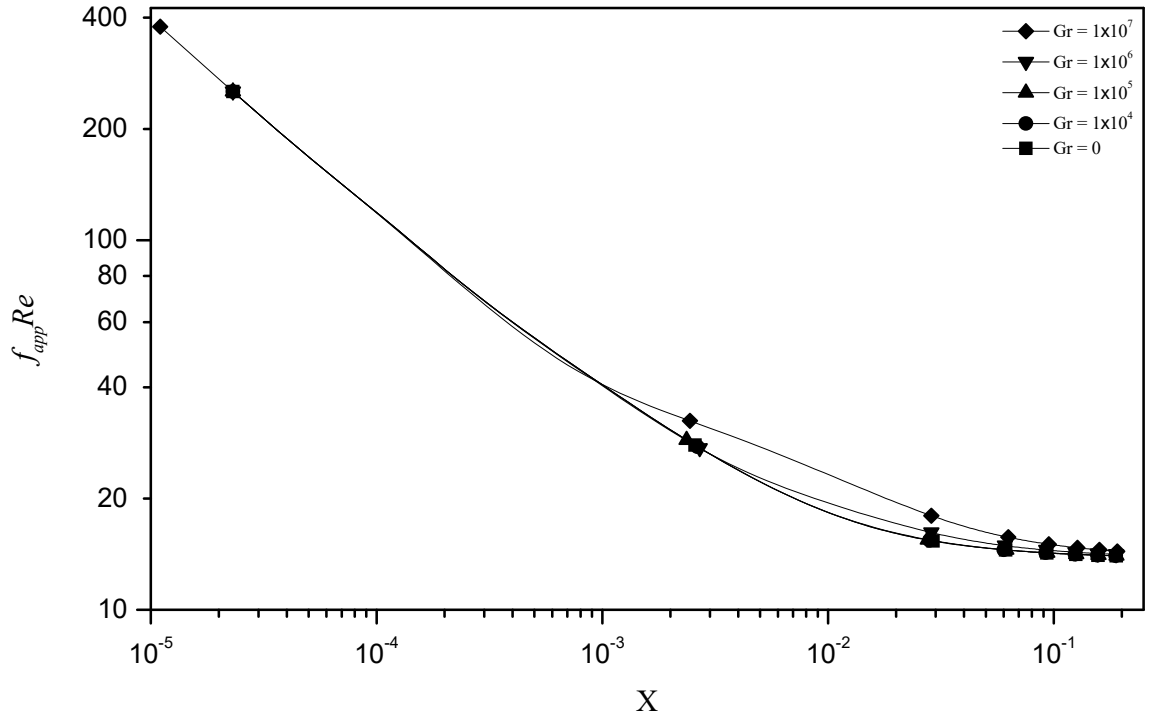

(d)

Fig. 9 Effect of Gr on the local heat transfer and flow parameters for circular sector duct mixed convection flow: (a) *Nu*, (b) *fRe*, (c) *Nu/fRe*, (d) *fappRe*

Open Science Index, Mechanical and Mechatronics Engineering Vol:15, No:3, 2021 publications.waset.org/10011918/pdf

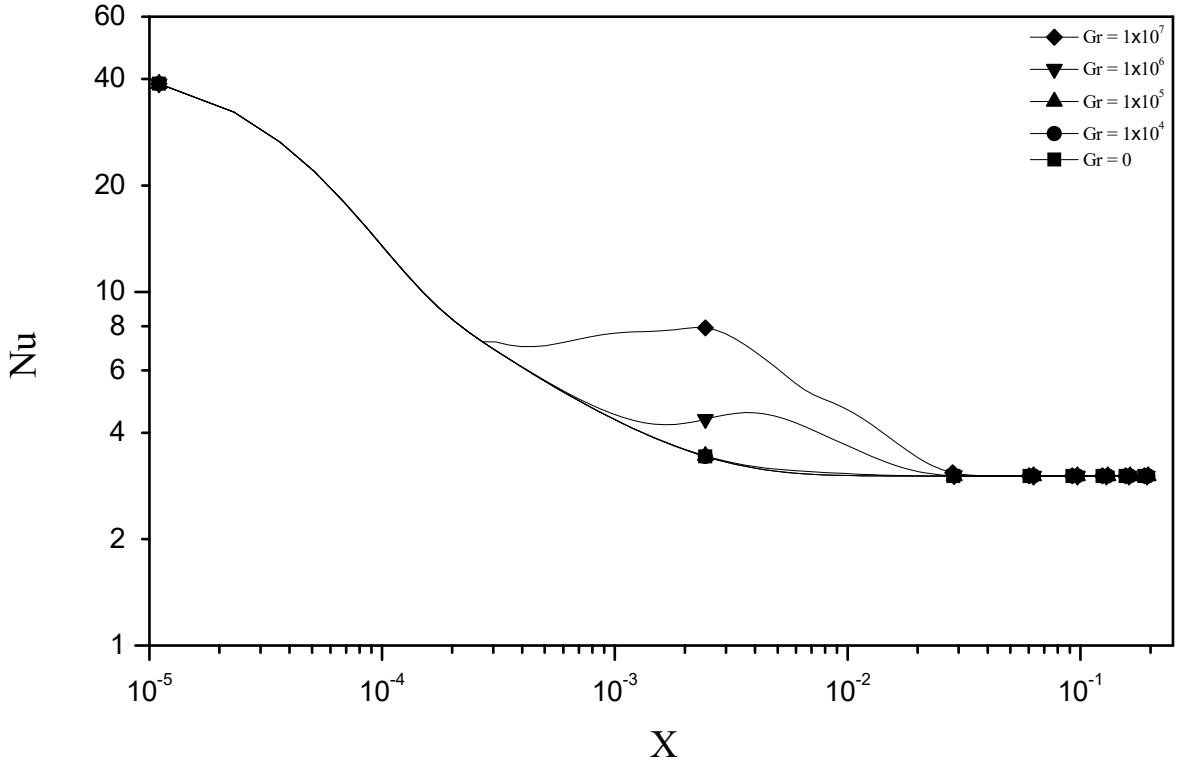

(a)

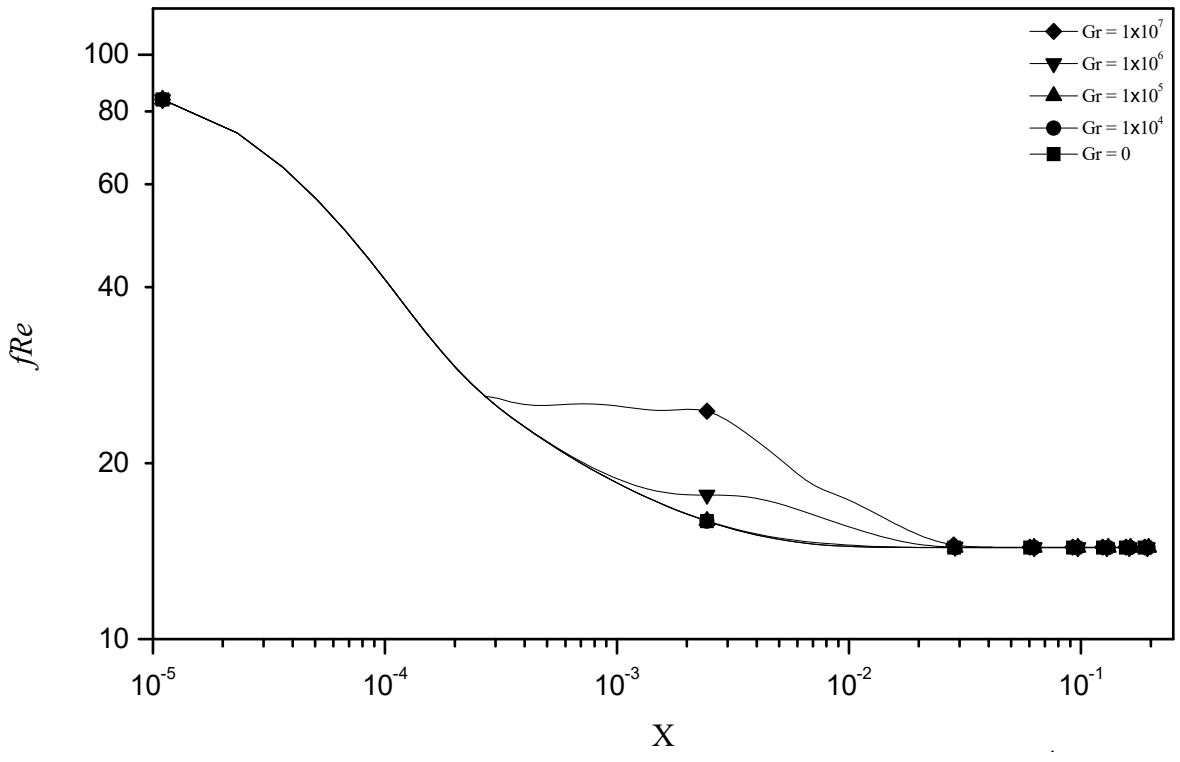

(b)

Open Science Index, Mechanical and Mechatronics Engineering Vol:15, No:3, 2021 publications.waset.org/10011918/pdf

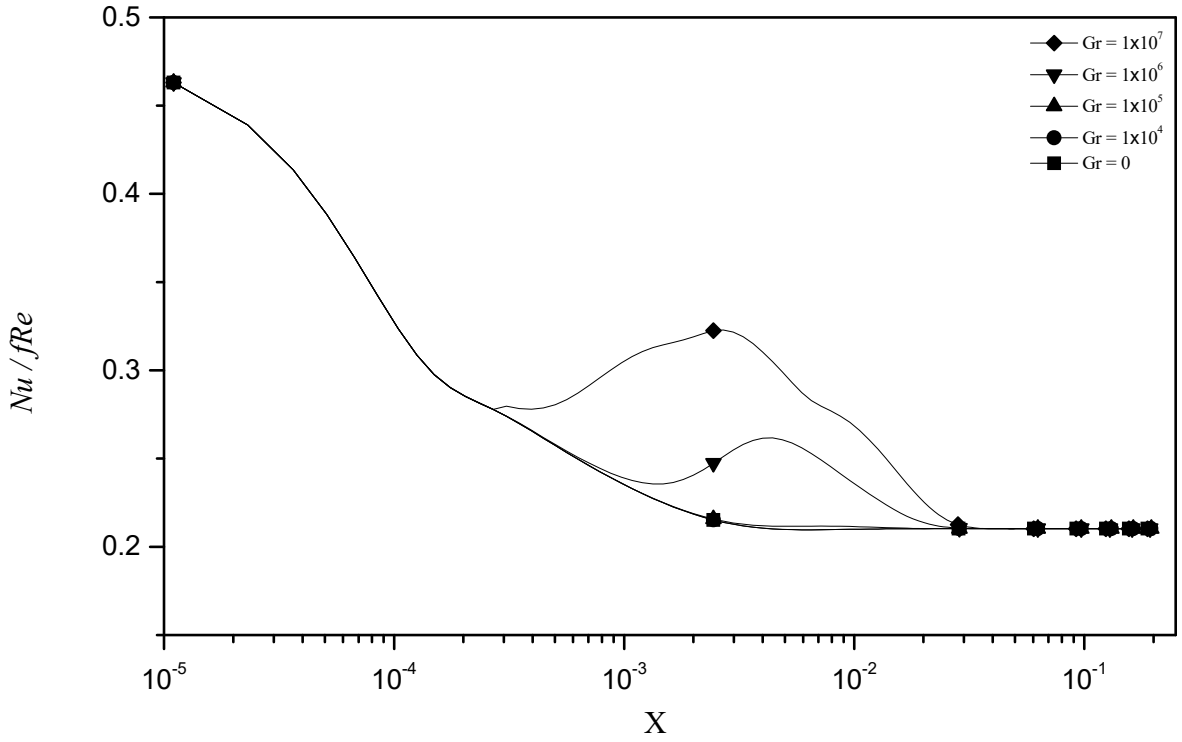

(c)

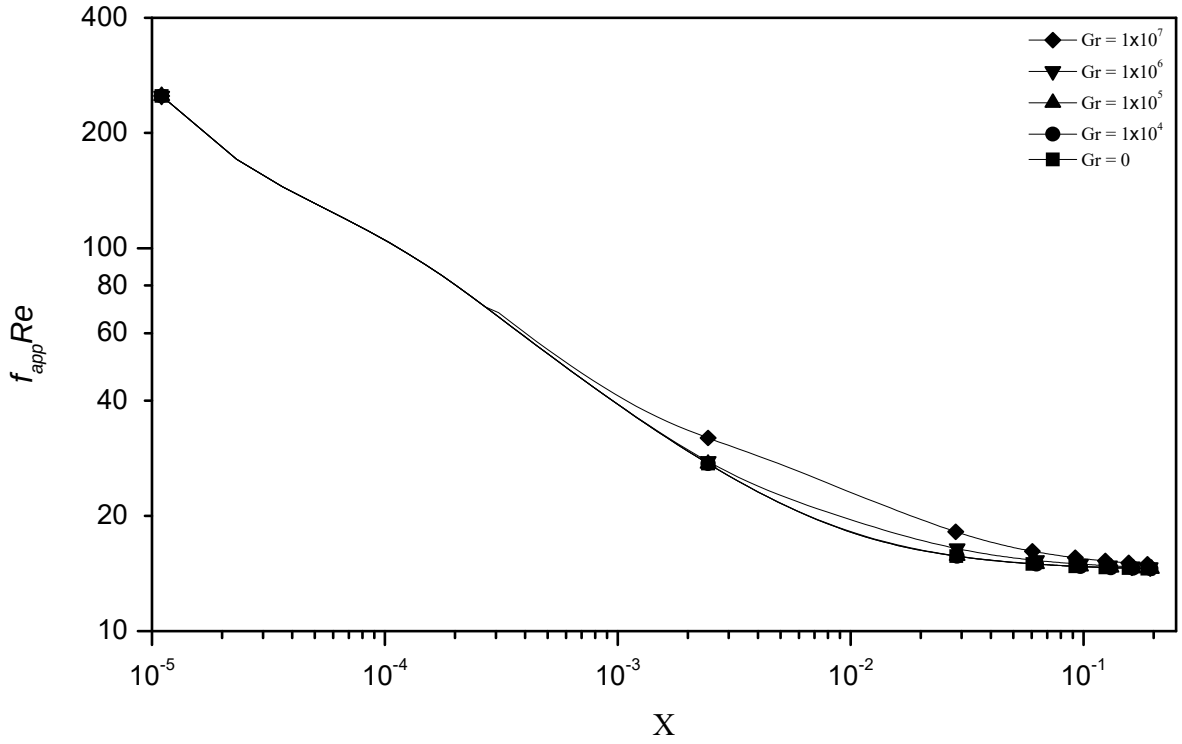

(d)

Fig. 10 Effect of *Gr* on the local heat transfer and flow parameters for annular sector duct mixed convection flow: (a) *Nu*, (b) *fRe*, (c) *Nu/fRe*, (d) $f_{app}Re$

For the product *fRe* as shown in Fig. 9 (b) when $Gr \geq 10^6$ *fRe* curve deviates from its forced convection counterpart in the developing region and rejoins it at a value of *13.7442* in the fully developed region. This indicates that the increased *Nu* in simultaneously developing mixed convection does not

come without penalty. However, Fig. 9 (c) shows that the ratio Nu/fRe increases as well and it is also important to note that the increase in the value of fappRe is substantially smaller than the corresponding increase in Nu as it can be seen from Fig. 9 (d). Similar behavior is observed for the annular sector duct case as shown in Fig. 10, however, the asymptotic values of Nu and fRe in the fully developed region are higher at 3.0168 and *14.3468*, respectively.

V. Conclusion

This numerical study is conducted on simultaneously developing combined free and forced convection for laminar flow in horizontal isothermal circular and annular sector ducts with $2\phi = \pi/4$. Results were limited to only one duct orientation and a Prandtl number of $Pr = 0.7$. Results show that the flow domain can be divided axially into three main regions, a near region where secondary flow is negligible, an intermediate region with mixed convection, and a far region with fully developed forced convection. The secondary flow in the intermediate region causes a significant change of the temperature and velocity profiles from those of pure forced convection which enhances the local heat transfer in some cases by up to 2.5 times from forced convection predictions and the enhancement increases as Grashof number increases.

References

[1] I.M. Rustum and H.M. Soliman, "Numerical analysis of laminar forced convection in the entrance region of tubes with longitudinal internal fins," *Journal of Heat Transfer*, vol. 110, no. 2, pp. 310–313, 1988.

[2] I.M. Rustum and H.M. Soliman, "Numerical analysis of laminar mixed convection in horizontal internally finned tubes," *International Journal of Heat and Mass Transfer*, vol. 33, no. 7, pp. 1485–1496, 1990.

[3] C.A. Hieber and S.K. Sreenivasan, "Mixed convection in an isothermally heated horizontal pipe," *International Journal of Heat and Mass Transfer*, vol. 17, no. 11, pp. 1337–1348, 1974.

[4] J.-W. Ou and K.C. Cheng, "Natural convection effects on Graetz problem in horizontal isothermal tubes," *International Journal of Heat and Mass Transfer*, vol. 20, no. 9, pp. 953–960, 1977.

[5] C.A. Hieber, "Mixed convection in an isothermal horizontal tube: some recent theories," *International Journal of Heat and Mass Transfer*, vol. 24, no. 2, pp. 315–322, 1981.

[6] M. Hishida, Y. Nagano, and M.S. Montesclaros, "Combined forced and free convection in the entrance region of an isothermally heated horizontal pipe," *Journal of Heat Transfer,* vol. 104, no. 1, pp. 153-159, 1982.

[7] M. Wang, T. Tsuji, and Y. Nagano, "Mixed convection with flow reversal in the thermal entrance region of horizontal and vertical pipes," *International Journal of Heat and Mass Transfer*, vol. 37, no. 15, pp. 2305–2319, 1994.

[8] B. Shome and M.K. Jensen, "Mixed convection laminar flow and heat transfer of liquids in isothermal horizontal circular ducts," *International Journal of Heat and Mass Transfer*, vol. 38, no. 11, pp. 1945–1956, 1995.

[9] A.R. Brown and M.A. Thomas, "Combined free and forced convection heat transfer for laminar flow in horizontal tubes," *Journal of Mechanical Engineering Science*, vol. 7, no. 4, pp. 440–448, 1965.

[10] C.A. Depew and S.E. August, "Heat transfer due to combined free and forced convection in a horizontal and isothermal tube," *Journal of Heat Transfer,* vol. 93, no. 4, pp. 380-384, 1971.

[11] W.W. Yousef and J.D. Tarasuk, "An Interferometric Study of Combined Free and Forced Convection in a Horizontal Isothermal Tube," *Journal of Heat Transfer*, vol. 103, no. 2, pp. 249–256, 1981.

[12] W.W. Yousef and J.D. Tarasuk, "Free Convection Effects on Laminar Forced Convective Heat Transfer in a Horizontal Isothermal Tube," *Journal of Heat Transfer*, vol. 104, no. 1, pp. 145–152, 1982.

[13] J.P. Coutier and R. Greif, "An investigation of laminar mixed convection inside a horizontal tube with isothermal wall conditions," *International journal of heat and mass transfer*, vol. 28, no. 7, pp. 1293–1305, 1985.

[14] C. Prakash and Y.-D. Liu, "Analysis of laminar flow and heat transfer in the entrance region of an internally finned circular duct.," *Journal of Heat Transfer,* vol. 107, no. 1, pp. 84-91, 1985.

[15] S.W. Hong, and A.E. Bergels, "Laminar flow heat transfer in the entrance region of semi-circular tubes with uniform heat flux," *International Journal of Heat and Mass Transfer,* vol. 19, no. 1, pp. 123-124, 1976.

[16] Q.M. Lei and A.C. Trupp, "Further analyses of laminar flow heat transfer in circular sector ducts," *Journal of Heat Transfer,* vol. 111, no. 4, pp. 1088-1090, 1989.

[17] Q.M. Lei and A.C. Trupp, "Maximum velocity location and pressure drop of fully developed laminar flow in circular sector ducts," *Journal of Heat Transfer*, vol. 111, no. 4, pp. 1085-1087, 1989.

[18] Q.M. Lei and A.C. Trupp, "Predictions of laminar mixed convection in a horizontal semicircular duct," in *Proceedings of the 6th International Symposium on Heat and Mass Transfer*, 1990, pp. 10–12.

[19] Q.M. Lei and A.C. Trupp, "Experimental study of laminar mixed convection in the entrance region of a horizontal semicircular duct," *International journal of heat and mass transfer*, vol. 34, no. 9, pp. 2361–2372, 1991.

[20] K.C. Karki, P.S. Sathyamurthy, and S. V Patankar, "Laminar mixed convection in a horizontal semicircular duct with axially nonuniform thermal boundary condition on the flat wall," *Numerical Heat Transfer*, vol. 25, no. 2, pp. 171–189, 1994.

[21] A.A. Busedra and H.M. Soliman, "Analysis of laminar mixed convection in inclined semicircular ducts under buoyancy-assisted and-opposed conditions," *Numerical Heat Transfer: Part A: Applications,* vol. 36, no. 5, pp. 527–544, 1999.

[22] A.A. Busedra and H.M. Soliman, "Experimental investigation of laminar mixed convection in an inclined semicircular duct under buoyancy assisted and opposed conditions," *International Journal of Heat and Mass Transfer*, vol. 43, no. 7, pp. 1103–1111, 2000.

[23] Y. El. Hasadi, I. Rustum, and A. Abdalla, "Laminar Mixed Convection in the Entrance Region of Semicircular Duct with Constant Heat Flux," In: *9th AIAA/ASME Joint Thermophysics and Heat Transfer Conference*, 2006, pp. 1-13.

[24] C. Chinporncharoenpong, "Combined convection in horizontal circular sector ducts of various cross-sectional orientations," 1993.

[25] C. Chinporncharoenpong, A.C. Trupp, and H.M. Soliman, "Laminar Mixed Convection in Horizontal Circular Sector Ducts," i*n International Heat Transfer Conference,*1994, pp. 447-452.

[26] R.K. Shah and A.L. London, *Laminar flow forced convection in ducts, Advances in heat transfer, supplement 1. Academic Press*, New York, 1978.

[27] H.S. Heaton, W.C. Reynolds, and W.M. Kays, "Heat transfer in annular passages. Simultaneous development of velocity and temperature fields in laminar flow," *International Journal of Heat and Mass Transfer*, vol. 7, no. 7, pp. 763–781, 1964.

[28] H.M. Soliman, "Laminar heat transfer in annular sector ducts," *Journal of Heat Transfer*, vol. 109, no. 1, pp. 247–249, 1987.

[29] T.M. Ben-Ali, H.M. Soliman, and E.K. Zariffeh, "Further results for laminar heat transfer in annular sector and circular sector ducts," *Journal of Heat Transfer*, vol. 111, no. 4, pp. 1090-1093, 1989.

[30] C.Y. Han and S.W. Baek, "Natural convection phenomena affected by radiation in concentric and eccentric horizontal cylindrical annuli," *Numerical Heat Transfer: Part A: Applications*, vol. 36, no. 5, pp. 473–488, 1999.

[31] N. Islam, U.N. Gaitonde, and G.K. Sharma, "Mixed convection heat transfer in the entrance region of horizontal annuli," *International journal of heat and mass transfer*. vol. 44, no. 11, pp. 2107–2120, 2001.

[32] D. Poulikakos and M. Kazmierczak, "Forced convection in a duct partially filled with a porous material," *Journal of Heat Transfer,* vol. 109, no. 3, pp. 653–662, 1987.

[33] M. Parang and M. Keyhani, "Boundary effects in laminar mixed convection flow through an annular porous medium," *Journal of Heat Transfer,* vol. 109, no. 4, pp. 1039-1041,1987.

[34] A. Haji-Sheikh, "Fully developed heat transfer to fluid flow in rectangular passages filled with porous materials.," *Journal of Heat Transfer,* vol. 128, no. 6, pp. 550–556, 2006.

Open Science Index, Mechanical and Mechatronics Engineering Vol:15, No:3, 2021 publications.waset.org/10011918/pdf

[35] K. Hooman and A.A. Merrikh, "Analytical solution of forced convection in a duct of rectangular cross section saturated by a porous medium.," *Journal of Heat Transfer,* vol. 128, no. 6, pp. *596-600, 2006.*
[36] C.Y. Wang, "Analytical Solution for Forced Convection in a Semi-Circular Channel Filled with a Porous Medium," *Transport in Porous Media*, vol. 73, no. 3, pp. 369–378, 2008.
[37] C.Y. Wang, "Analytical Solution for Forced Convection in a Sector Duct Filled With a Porous Medium," *Journal of Heat Transfer,* vol. 132, no. 8, 2010.
[38] V.K. Verma and S. Datta, "Flow in an annular channel filled with a porous medium of variable permeability," *Journal of Porous Media*, vol. 15, no. 10, pp. 891–899, 2012.
[39] M. Iqbal and H. Afaq, "Fluid flow and heat transfer through an annular sector duct filled with porous media," *Journal of Porous Media*, vol. 18, no. 7, pp. 679-687, 2015.
[40] M. Nasiri, S.G. Etemad, and R. Bagheri, "Experimental heat transfer of nanofluid through an annular duct," *International Communications in Heat and Mass Transfer*, vol. 38, no. 7, pp. 958–963, 2011.
[41] M.H. Shedid, "Computational heat transfer for nanofluids through an annular tube," in *Proc, the International Conference on Heat Transfer and Fluid Flow*. *Prague, Czech Republic,* 2014, pp.206:1-10.
[42] A. Beheshti, M.K. Moraveji, and M. Hejazian, "Comparative numerical study of nanofluid heat transfer through an annular channel," *Numerical Heat Transfer, Part A: Applications*, vol. 67, no. 1, pp. 100–117, 2015.
[43] F. Ahmed, M. Iqbal, and P. Ioan, "Numerical simulation of forced convective power law nanofluid through circular annulus sector," *Journal of Thermal Analysis and Calorimetry*, vol. 135, no. 2, pp. 861–871, 2019.
[44] F. Ahmed and M. Iqbal, "Heat Transfer Analysis of MHD Power Law Nano Fluid Flow through Annular Sector Duct," *Journal of Thermal Science*, vol. 29, no. 1, pp. 169–181, 2020.
[45] S. V Patankar and D.B. Spalding, "A calculation procedure for heat, mass and momentum transfer in three-dimensional parabolic flows," in *Numerical prediction of flow, heat transfer, turbulence and combustion*. Elsevier, 1983, pp. 54–73
[46] W. M. Kays, *Convective Heat and Mass Transfer.* New York: McGraw-Hill, 1966, pp. 62.
[47] S. Patankar, *Numerical heat transfer and fluid flow.* Taylor & Francis, 2018.

Open Science Index, Mechanical and Mechatronics Engineering Vol:15, No:3, 2021 publications.waset.org/10011918/pdf